Tabebuia Rosea (family Bignoniaceae) Flower Extraction and its Antioxidant Activity: Green Synthesis of Iron Oxide Nanoparticles

K.Devika[1] , G.Anburaj[2], R.Sathish kumar[3], R.Manikandan[4]

[1,4,] Department of Chemistry, A.V.V.M.S.P College, (Affiliated to Bharathidasan University-Tiruchirappalli), Thanjavur, Tamil Nadu, India

[2]Department of Chemistry PRIST Deemed to be University Thanjavur Tamil Nadu, India

[3,] Department of Botany, Jamal Mohamed College (Autonomous) (Affiliated to Bharathidasan University-Tiruchirappalli), Tamil Nadu, India

Contact corresponding auther devikasaravanan727@yahoo.com cell +919715392903

Abstract:

To evaluate the antibacterial and antifungal benefits of iron nanoparticles (FeNP) on an assortment of pathogenic microorganisms, we extracted the aqueous flower extract of Tabebuia rosea. The ratio of precursors to flower extraction was 1:1. Different concentrations of iron sulfate and flower extraction were employed. The findings revealed dependencies on the synthesis conditions and FeNP particle size. because there is a direct correlation between the circumstances of production along with a rise or reduction of the antimicrobial activity, the activity of the antimicrobial was then assessed against microbes in their Finally, the total flavonoids and overall polyphenols were quantified, as well as the antioxidant capacity of the Tabebuia rosea extract was determined, enabling the antimicrobial activity of the FeNPs to be linked to the extract's constituents and also docking Alpha-amylase glucosidase Frequency of amino acid and Fe^{3+} & Fe^{2+} binding affinity was calculated.

Keywords: *Tabebuia rosea* Family Bignoniaceae iron nanoparticles, SEM with EDAX XRD, antibacterial and antifungal, molecular

1. Introduction

A particle of matter having a diameter of one to one hundred nanometers (nm) is commonly referred to as a nanoparticle or ultrafine particle.[1-2] When referring to fibers and tubes whose diameters are smaller than 100 Angstroms in only two dimensions or larger particles up to 500 nm, the expression is occasionally used.[3] The neotropical tree Tabebuia rosea, frequently referred to as the pink pout and rosy trumpet tree[4], can grow as tall as 30 m (98 ft) and as broad as 100 cm (3 ft) at breast height. In Costa Rica, the term roble de sabana, which translates to "savannah oak," is frequently used. This is likely because the plant is frequently found in severely deforested areas and its wood resembles that of oak trees. For getting rid of uterine cancer, malaria, and intestinal parasites, preparations of the tree's bark are swallowed. Anaemia, also known as constipation can both be treated with a bark decoction. The flowers, leaves, and roots have been used to make a decoction that has been used to cure tonsil irritation, induce sweating, lower fevers, and alleviate discomfort. [5] Lapachol, a naturally occurring organic substance identified from different other *Tabebuia species*, is one of the numerous phytochemicals that are active in the tree.[6] Terabit magnetic storage devices, catalysis, sensors, superparamagnetic relaxometry, magnetized particles imaging, magnetic fluid hyperthermia, separation of biomolecules, and targeted drug and gene delivery for medical diagnosis and therapeutics are just a few uses for iron oxide nanoparticles. For these uses, coating the nanoparticles with substances like long-chain fatty acids, alkyl-substituted amines, and diols is necessary. They have been used in dietary supplement formulations.[7] Nanoparticles (NPs) are increasingly used to target bacteria as an alternative to antibiotics. Nanotechnology may be particularly advantageous in treating bacterial infections. (8) Antifungal activity was observed by inhibiting spore germination and determining the zone of inhibition of fungal pathogens caused by different concentrations of iron oxide nanoparticles in the culture media. It was observed from the present study that Fe2O3 nanoparticles showed significant antimycotic activity against all fungal pathogens tested. (9) Inorganic nanoparticles such as CeO3, TiO2, and Fe3O4 act as a platform for their excellent performance in antioxidant effect. They may offer the potential for further development due to their small and controllable sizes, flexibility for modification, relatively low toxicity, and ease of preparation. (10)

2. Materials and Methods

2.1 Plant material and preparation of the extract

extract of liquid water from its source. A plants extract was used to prepare the H2O extracts. To make sure they were clean, they were gathered and given a thorough wash with distilled water. Fresh bark, weighing about 20 g, was pounded in a mortar and crusher. Twenty milligrams of TRP powders were cooked for 20 minutes in 100 ml of deionized water before being swirled magnetically at 60 °C and processed with filter paper. For future usage, the extract was kept in the refrigerator. The TRP extract has been broken into very small pieces of plant parts, properly cleaned with distilled water, and vacuum-dried after being collected in the amount of 100 g. Dried 8.3 g of dried TRP was removed utilizing 125 milliliters of DD H2O for 30 minutes at 60° C. Before filtration, the mixture was allowed to cool. The material had been spun at 12000 revolutions per minute for 30 minutes after extraction. Before use, the final product was collected, filtered, and kept at -20 °C.(11).

2.2. Biosynthesis of Iron Nanoparticles (FeNPs).

FeCl3 has been dispersed in 40 mL of deionized water to create TRP-FeNP. A 0.1 M solution of FeCl3 was made. Aqueous SLE and a 0.1 M iron chloride solution were combined in a 2:1 proportion of volume and stirred continuously with magnetic stirring at 60 degrees Celsius for 30 minutes to create FeNPs. Fe+3 ion depletion results in the appearance of black color. The highest UV/visible absorption spectra of FeNPs in reaction mixtures generated in a 2:1 ratio were noted. A 0.1 M ferric chloride solution and water BPE (supernatant at room temperature) were combined in a 2:1 ratio of volumes to create BPE-FeNPs. From that, it was given a minute's worth of handshaking before being left standing at ambient temperature for an hour. After 10 minutes, the solution's coloration transformed between clear yellow to dark black, and this was seen and noted. The mixture was centrifuged at 12000 rotations per minute for 30 minutes, and the supernatant was drained out. The residual biomolecules in the black paste were dispersed again in ethanol before being washed with ultrapure water. To completely purify the NPs, centrifugation, and redispersion in ethanol and ultrapure water were performed three times. The light black paste was then packed, stored, and oven-dried for an additional night at 60° C [12].

2.3. Characterization of Biosynthesized Iron Nanoparticles

2.3.1. Characterization of FeNPs

Several methods such as ultraviolet-visible spectroscopy (UV-Vis), Fourier transform infrared spectroscopy (FTIR), scanning electron microscopy, energy dispersive X-ray spectroscopy, X-ray diffraction (XRD), and particle size analyzer Using FeNPs.

2.3.2. UV-Vis Analysis.

Changes in the reaction mixture were visually observed and recorded. The samples were then examined spectrophotometrically in the UV-Vis range. The wavelength was scanned from 200 nm to 700 nm at 1 nm intervals.[13]

2.3.3. FTIR Analysis.

Measurements were performed using an FTIR system. Extractive functional groups that may have played a role in the synthesis of the iron microstructure were identified using his FTIR scan of iron NPs from *TRP* extract. A transmission mode range of 400–4000 cm-1 was used for the FTIR analysis.[14]

2.3.4. Scanning electron microscopy (SEM-EDX)

Scanning electron microscopy (JSM-IT 500, Jeol, Boston, MA, USA), was used to examine the nanoparticles and establish their surface shape.[15] The grain structure was analyzed using SEM equipment (JEOL, USA). Before analysis, the nanoparticles were extensively washed with ethanol to remove any impurities that might have been present.[16] The powdered samples were then dispersed in ethanol using ultrasound, followed by filtration. Samples

were finally dried and coated with a (10-15) nm layer of high-purity gold before analysis. Observation by SEM was performed at a fixed electron beam output of 30 kV and a working distance of 11 mm. EDX (energy dispersive X-ray) analysis was performed to confirm the elemental content in the nanoparticles. The samples were analyzed by SEM-EDX at 30 kV and the EDX spectra had an acquisition time of 100 seconds.

2.3.5. XRD Analysis.

We used an X-ray diffractometer to study crystalline metallic iron NPs. The instrument used 45 kV Cu-Kα radiation and a monochromatic filter with a wavelength range of 20-80 degrees. The biosynthesized FeNPs were completely dried in powder form before stacking on the XRD apparatus cube.[17]

2.3.6. Antibacterial Potential.

The antibacterial activity of living FeNPs from *trp* was tested using the agar diffusion method against two bacterial strains: Bacillus subtilis (MTTC 1133) and Escherichia coli (MTTC 62) from the Microbial Type Culture Collection and Gene Bank (MTCC). Chandigarh, India, and the zone of inhibition were measured in millimeters using the agar-well diffusion method described in [18]. Antibiotics such as chloramphenicol and gentamicin were used as positive controls in this study.

2.7 DPPH Radical Scavenging Assay

The antioxidant assay of FeNPs from *trp* was used against DPPH radical and was determined by UV spectrophotometry at 517 nm. This activity was measured according to the method previously performed [19]. Five different concentrations (100–500 μg/ml) of plant extracts were prepared. Ascorbic acid was used as a standard. 1 ml from each extract and 3 ml of each solvent were mixed with 0.5 ml of 1.0 mM DPPH in methanol and allowed to react at room temperature for 30 minutes. The same amount of solvent and DPPH to prepare the blank solution which is a control. The sample was prepared in triplicate value for each analysis and the mean value of the absorbance was noted. The DPPH radical scavenging was calculated by the following formula:

DPPH inhibition percentage = [(A0-A1)/A0] x 100

Where, A0 - Absorbance of the control, Al - Absorbance of the FeNP/ascorbic acid.

The inhibitory concentration (IC50) of the plant extract was reported as the number of antioxidants required to reduce the initial DPPH concentration by 50%. A triplicate test was performed and graphs were plotted using the average of three determinations.

2.8 METHODS OF MOLECULAR DOCKING

As an updated version of MIB, MIB2 offers a total of 18 types of metal ions (Ca^{2+}, $Cu2^{2+}$,, $Fe^{3+,}$ $Mg^{2+,}$ Mn^{2+}, Zn^{2+}, Cd^{2+}, Fe^{2+}, Ni^{2+}, Hg^{2+}, Co^{2+}, Cu^{2+}, Au^{2+}, Ba^{2+}, Pb^{2+}, Pt^{2+}, Sm^{3+} and Sr^{2+}), supportive of binding site predictions. Both prediction systems use the fragment transformation method. (Lu et al., 2022)

3 Results and Discussion

3.1 Characterization of Fe-NPs-Tr flower

The identity of the synthesized iron nanoparticles was established using the following analytical methods

3.2 XRD analysis

The crystallinity of FeNPs was assessed using XRD diffraction patterns. Figure c depicts the diffractogram's pattern. To achieve this outcome, iron nanoparticle production was permitted. Green-Synthesized FeNPs' XRD spectra. The diffraction peaks at 2 values of 30.2944, 35.668, 43.2994, 53.8234, 57.2722, 62.9664, and 74.6793, which are equivalent to the amorphous structure(220), (311), (400), (422), (511), (440), as well as (533) planes of cubic crystal system of iron oxide (Fe3O4), show that the FeNPs are truly crystalline. The purity of the synthesized FeNPs is indicated by the fact that the position and relative intensities of the diffraction peaks are identical to the standard information for bulk hematite (JCPDS file No. 96-900-5842). Our XRD results confirm those previously reported results. (21-23)

3.3 SEM and EDX analysis

A scanning electron microscope was used to determine the shape of ***Tabebuia rosea-capped*** FeO NPs (Fig. a). SEM images were seen in different magnification ranges like 2 µm–200 nm which demonstrated the presence of spherical-shaped nanoparticles with a mean average diameter of 70 nm. (24) The presence of carbon in trace amounts indicates the involvement of plant phytochemical groups in the reduction and capping of the synthesized ZnO NPs [25]

Elemental composition

The EDX analysis of Fe NPs-JF (Fig. d), which showed unique peak patterns due to C, O, Cl, and Fe, corroborated the elemental composition of the compound. According to EDX examination, the following weight percentages were found: C-32.32%, Fe,-43.25%, O-11.03%, Ca -8.30%, k-2.94%, P-1.21%, Cl-0.84%, Al-0.15%. The organic material generated from the mango peeling extraction was absorbed on the outside or close to tiny particles, as seen by the peaks for carbon and oxygen. [27].

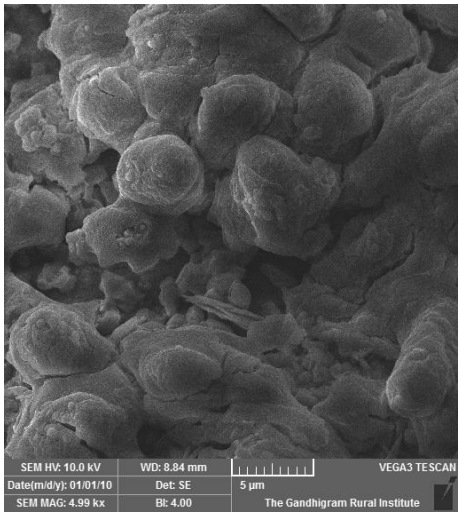

(a)

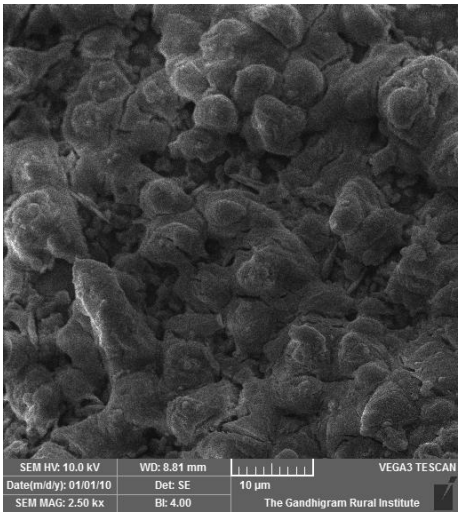

(b)

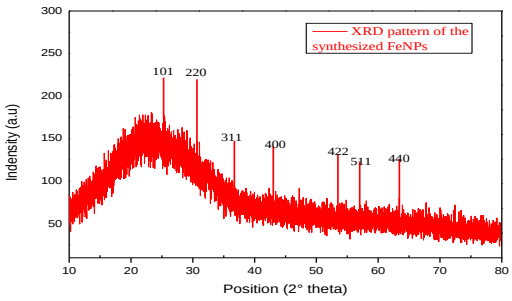

(c)

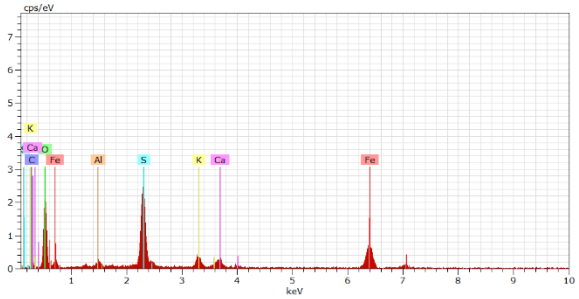

cps/eV

3.0

(d)

Figure 1. Characterization of the iron oxide nanoparticle ***Tabebuia rosea*** (**a**) SEM analysis with 5K, (**b**) SEM analysis with10K, (**c**) XRD analysis, (**d**) EDX analysis.

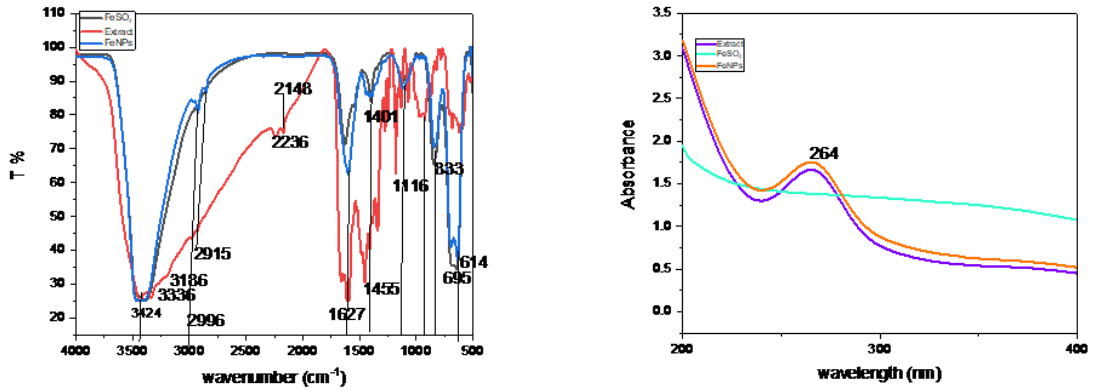

(a) **(b)**

Figure 2. (a) IR spectrum of (A) and iron oxide nanoparticle ***Tabebuia rosea*** (B); (b) UV-Vis spectra of FeCl3 and iron oxide nanoparticle ***Tabebuia rosea***

3.4 FeNPs of Antibacterial activity, Antifungal activity

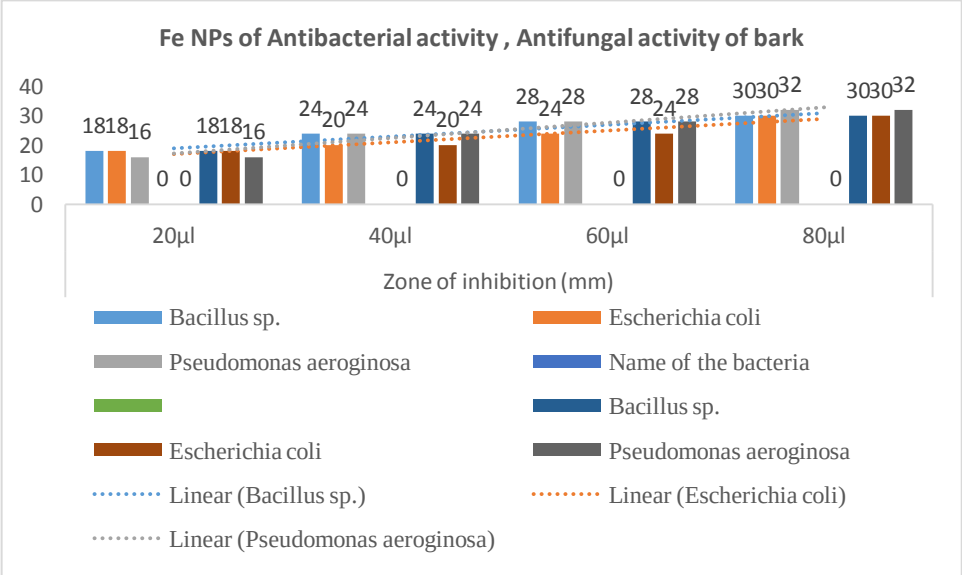

Table:18 Fe NPs of Antibacterial activity, Antifungal activity *Tabebuia rosea*

Name of the bacteria	**Zone of inhibition (mm)**			
	20µl	**40µl**	**60µl**	**80µl**
***Bacillus* sp.**	**18**	**24**	**28**	**30**
Escherichia coli	**18**	**20**	**24**	**30**
Pseudomonas aeroginosa	**16**	**24**	**28**	**32**

Name of the bacteria	Zone of inhibition (mm)			
	20µl	40µl	60µl	80µl
***Bacillus* sp.**	**18**	**24**	**28**	**30**
Escherichia coli	**18**	**20**	**24**	**30**
Pseudomonas aeroginosa	**16**	**24**	**28**	**32**

3.5 UV–Visible spectroscopy analysis

Figure b displays the iron biosynthetic nanoparticles' UV-Vis spectrum. Using UV-Vis spectroscopy, the surface resonance plasmon (SPR) of the FeNPs was completed. The synthesis of FeNPs is authorized by the peak frequencies at 264, 200–400 nm. The existence of the mentioned band, in contrast to earlier observations, supports the production of iron nanoparticles. (24-25)

3.6 FT-IR analysis

Fig. a displays the FT-IR taken from the green synthetic FeNPs T.r flower. The peaks around 700 and 400 cm-1 are typically caused by the vibration of metal nanoparticles in FT-IR analysis. 3424 IS INDICATE NH2; Carbonyl C=O stretching band; O-H stretching mode, 3336 aliphatic primary amines, 3186 0-H stretching, 2915C-H alkane, 2148 carbodiimide N=C=N,2926 -C-H symmetric stretching of –CH,2236 CΞN nitrile 1627 Amide I α – helical structure (C=O),1458 CH2 bend; P-O- anti-symmetric stretch,836 C=C Alken, The peaks at 614 and 695 cm-1, The peaks at 474.49 cm^{-1}, 621.08 cm^{-1} and 678.94 cm^{-1} ensure the presence of Fe–O bond in the sample (26-27). The peaks at the position of 3357.57 cm^{-1} represent the –OH bond stretching from the aqueous phase. Again, the peaks at 1433.11 cm^{-1}, and 3691.57 cm^{-1} also represents the –OH bond stretching and bending from various phenolic and carboxylic group respectively present in the plant extract (28). The FT-IR spectra of the Z. clip- divides sample and FeNPs were found to be comparable, providing evidence that iron nanoparticles were produced synthetically. The FTIR spectrum of iron oxide nanoparticles is shown in Fig. a. The bands at 2923 cm-1 and 2853 cm -1 are due to aromatic and aliphatic C-H stretching which suggests the presence of traces of oils or wax. The characteristic metal-oxygen bond formation is observed in the region of 400-850 cm-1. Peaks at 618cm−1 and 467cm-1 correspond to the stretching vibration of Fe–O. (29)

3.7 Antioxidant and cytotoxicity properties of FeNPs

Utilizing the DPPH method as a prevalent free radical test in this study, we evaluated the antioxidant capabilities of FeNPs that were T.r flowers extracted from water green-synthesized FeNPs. Oxidation is the transfer of electrons from one atom to another and is a component of aerobic metabolism in living things. In the body's ATP (adenosine triphosphate)-producing electron transport mechanism, oxygen serves as the electrons' recipient.

Tabebuia rosea had the highest activity, followed by *Tabebuia argentea* respectively. At the concentration of 1000 µg/mL, the scavenging activity of methanol extract reached 89.92%, but at the same concentration, that of Tabebuia argentea extracts was 72.88% respectively. It was evident that the Tabebuia rosea extracts showed proton-donating ability and this could serve as free radical inhibitors or scavengers, acting possibly as primary antioxidants. (30)

Concentrations (µg/ml)	% of inhibitions	
	Bark FeNPs	Standard as Ascorbic acid
100	17.27	24.12
200	32.62	40.46
300	53.6	61.37
400	68.92	80.55
500	72.88	91.82
IC_{50} Value	266.28**(µg/ml)**	245.34**(µg/ml)**

Figure: 3 **DPPH radical scavenging activity of *Tabebuia rosea* bark at different concentrations**

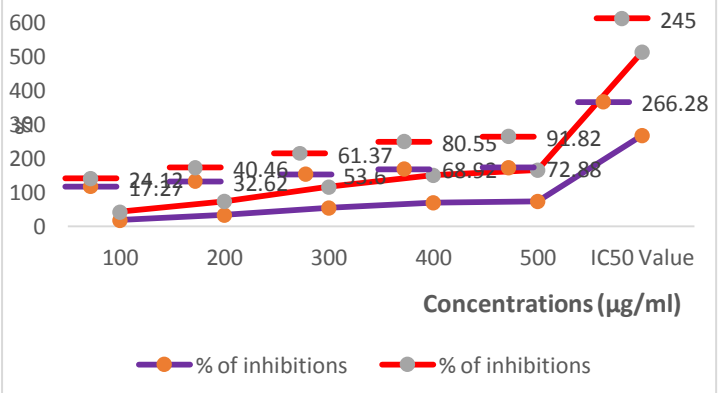

3.9 Alpha-amylase / glucosidase Frequency of amino acid and Fe^{3+} & Fe^{2+} binding affinity

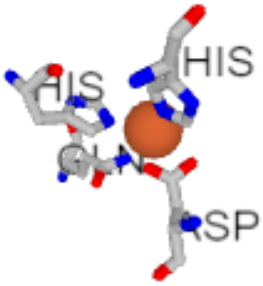

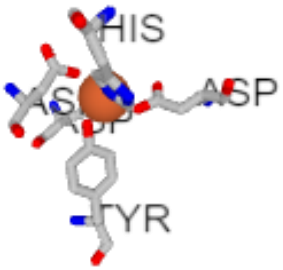

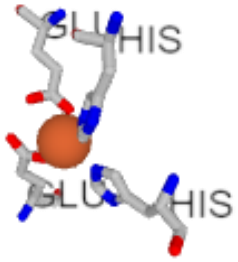

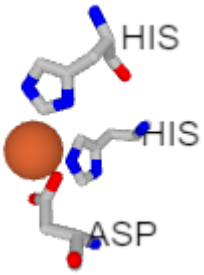

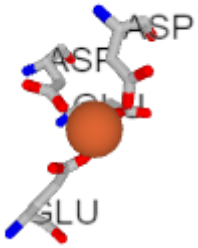

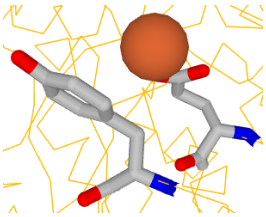

H-Histidine	D-aspartic acid	E-glutamic acid	L-leucine	S-serine	R-arginine	A-alanine	Q-glutamine	P-proline
16	17	17	4	4	3	1	3	0
30	19	12	2	4	6	1	4	1

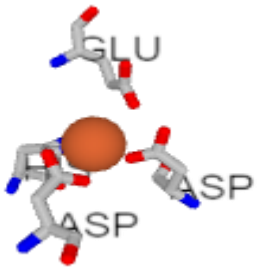

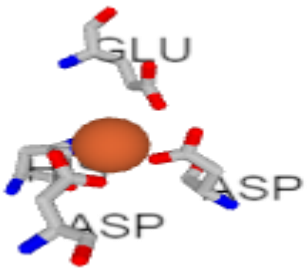

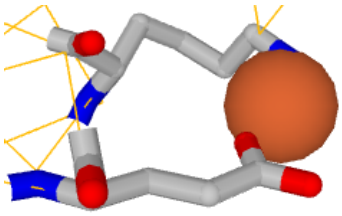

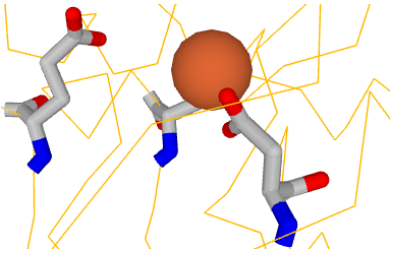

H-Histidine	D-aspartic acid	E-glutamic acid	L-leucine	S-serine	R-arginine	A-alanine	Q-glutamine	P-proline
51	30	17	4	13	6	10	3	2
12	16	5	1	13	5	0	1	0

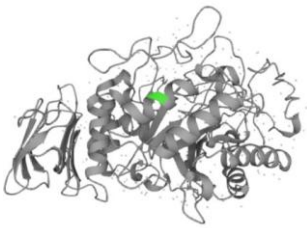

alpha-amylase- P56634

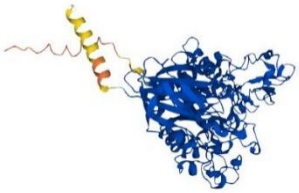

alpha-glucosidase Q95WY5

A performance comparison between MIB and MIB2 benefits from more protein structures becoming available since the development of MIB. For each type of metal ion, the numbers of binding templates in MIB2 range from 1.24 to 10.72 times the numbers in MIB. (31) The propensity of various protein and atom types on binding A greater likelihood of type 2 diabetes is linked to excess iron preservation and may harm pancreatic -cells and promote resistance to insulin via enhanced oxidative stress 22. The primary method of storing iron in the body is ferritin, which is a crucial protein that controls iron homeostasis. (Liu et al., 2020) In general, the molecular docking tests provided insight into the divided molecules' possible inhibiting the enzyme alpha and potential methods for the structure-based design or enhancement of such compounds or novel compounds. (Etsassala et al., 2022) This result is showing the many amino acids and is also given in table ( )high binding energy is histidine Fe2+(51) lowest binding is 2, and Fe3+ binding energy is 12 (H-Histidine) lowest binding energy 5 list H-Histidine, D-aspartic acid, E-glutamic acid, L-leucine, S-serine, R-arginine, A-alanine, Q-glutamine, P-proline alpha amylase-en P56634(Enzymes are protein), alpha-glucosidase Q95WY5(Enzymes are protein) this protein is more active with Fe2+ so finally we try to clinical work then confirmed.

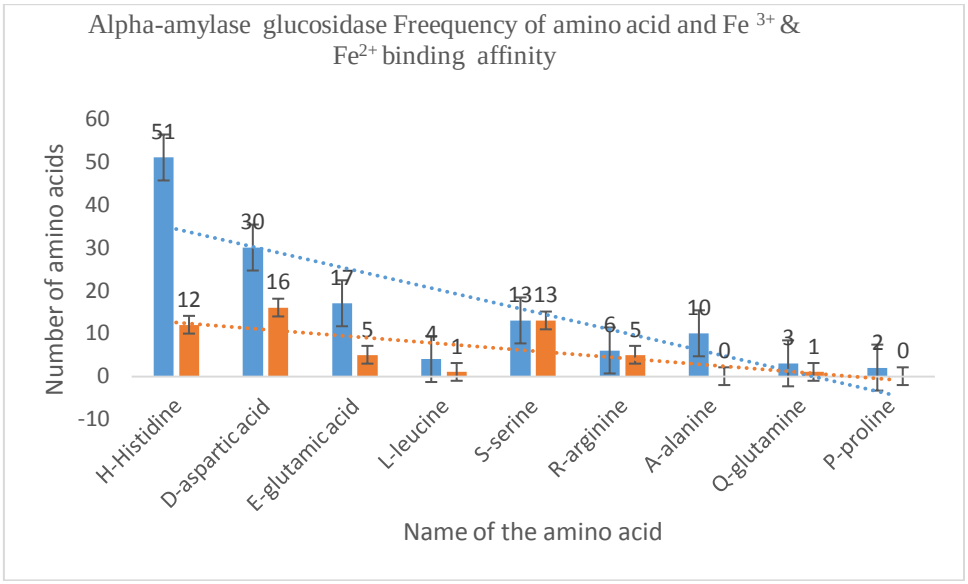
Alpha-amylase glucosidase Freequency of amino acid and Fe 3+ & Fe2+ binding affinity
Number of amino acids
60
50
40
30
20
10
0
-10
51
12
30
16
17
5
4
1
13
13
6
5
10
0
3
1
2
0
H-Histidine
D-aspartic acid
E-glutamic acid
L-leucine
S-serine
R-arginine
A-alanine
Q-glutamine
P-proline
Name of the amino acid

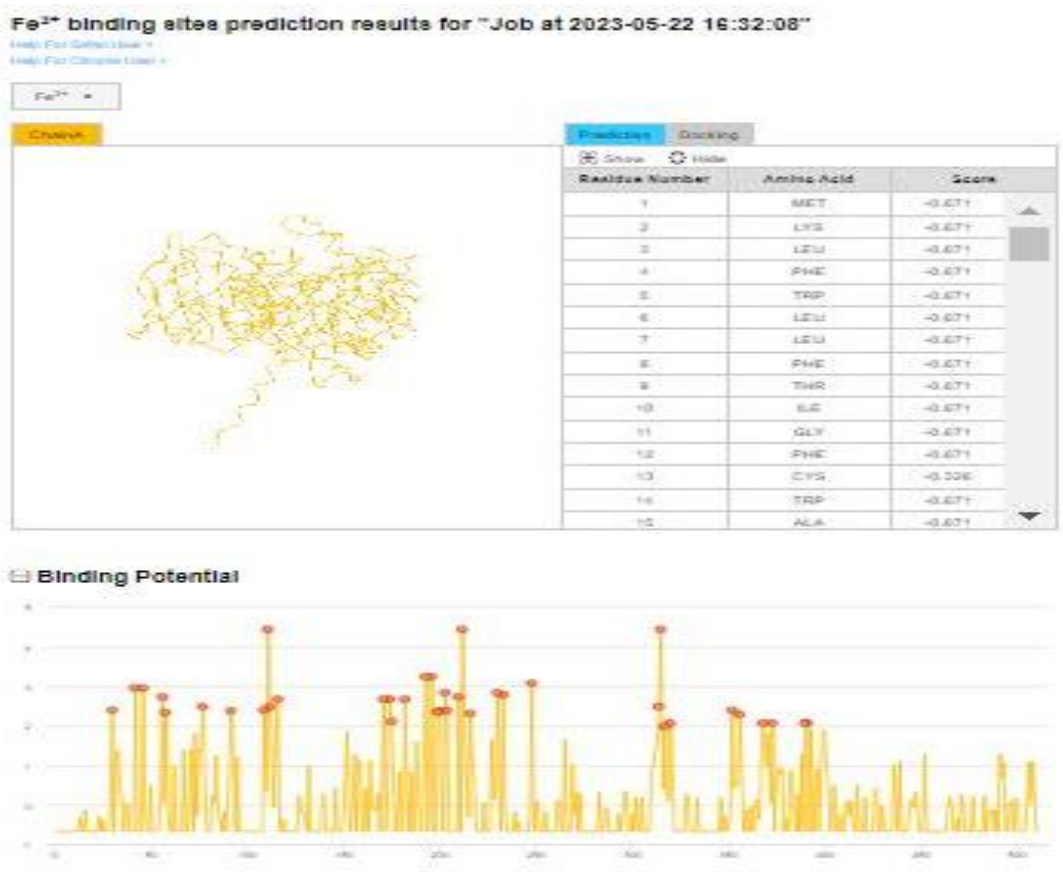
Fe³⁺ binding sites prediction results for "Job at 2023-05-22 16:32:08"
Residue Number
Amino Acid
Score
Binding Potential

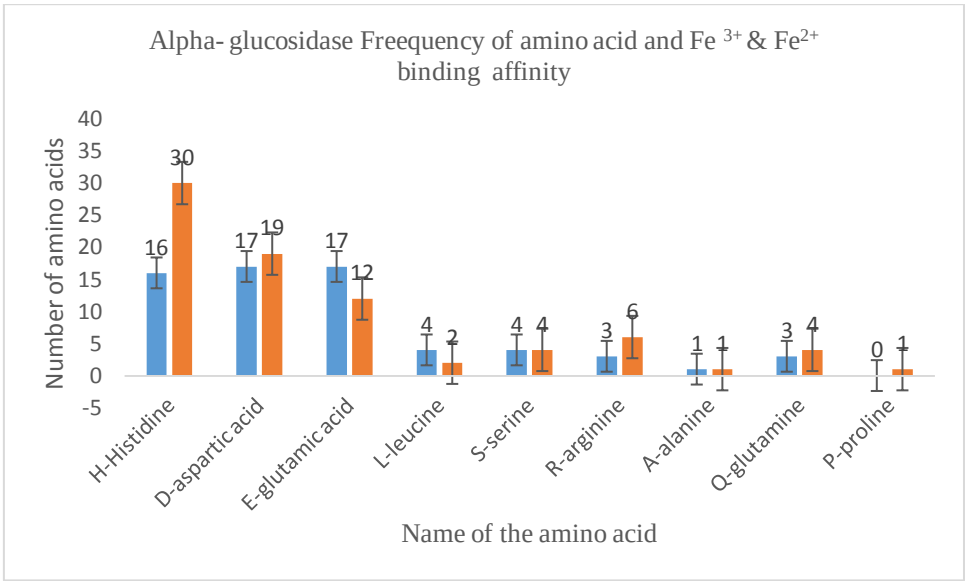

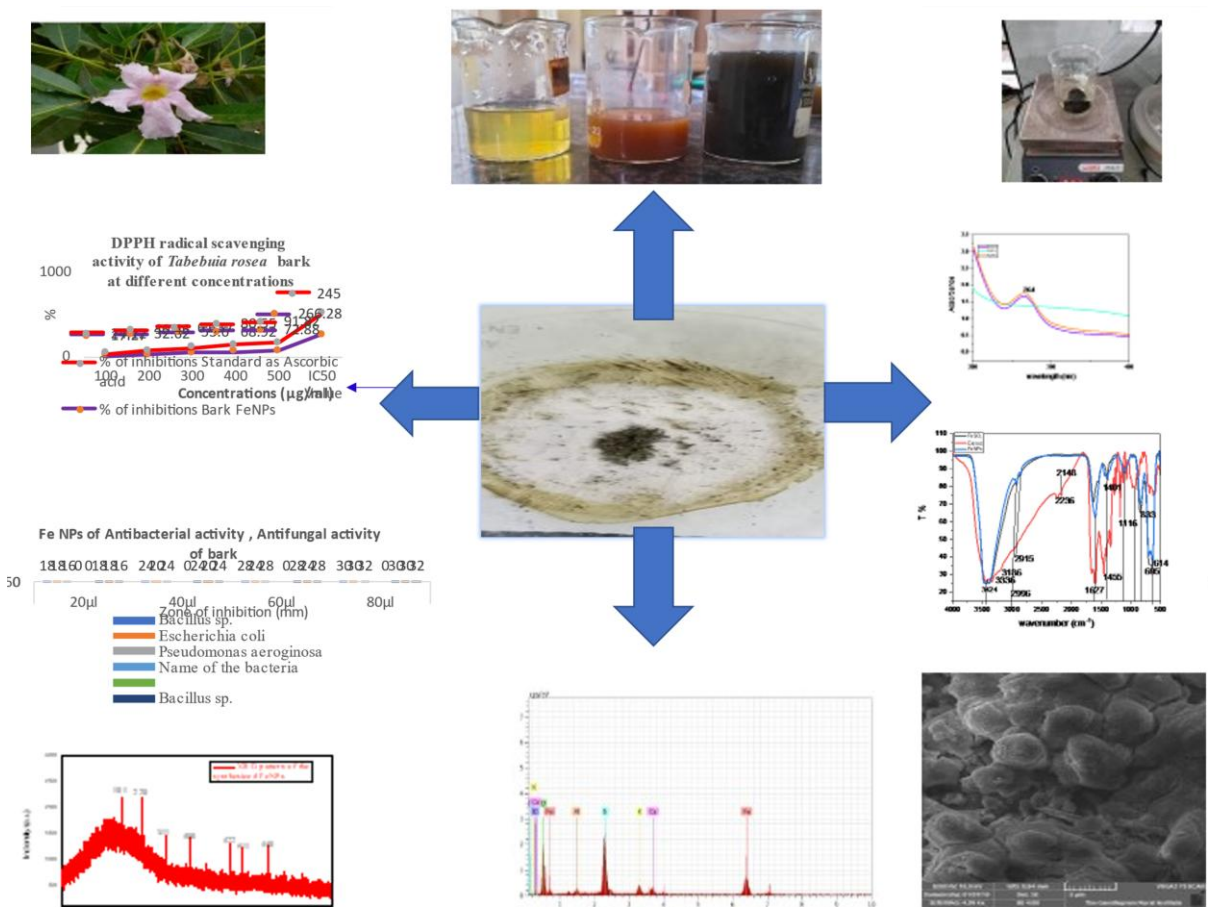

4. Conclusions

The synthesis of FeNPs using the *Tabebuia rosea* flower is effective, affordable, and safe for the environment. To throw light on the operation, equilibrium, and size of FeNPs generated in green, a few microscopic and spectroscopic methods have been used to investigate the NPs. Data Availability FeNPs were produced as crystalline and spherical nanoparticles. These FeNPs were also tested for their ability to fight bacterial and fungal stains with antibacterial efficiency. Positive and dependent-on-concentration outcomes were obtained. Additionally, It has been shown that polyphenols' beneficial effects depend on concentration. Finally, we did the molecular docking with the receptor Alpha-amylase and alpha-glucosidase it show the great result of molecular docking FeNPs are capable of both therapeutic and preventive microbial defense. This study further supported the antidiabetic & anticancer activity of *Tabebuia rosea* bark and flower extract. Further clinical studies are required to confirm its therapeutic efficacy.

Conflicts of Interest

The authors declare that there are no conflicts of interest.

Funding

This research received no external funding.

4 References

1. U.S. Environmental Protection Agency (): "Module 3: Characteristics of Particles Particle Size Categories". From the EPA Website.
2. Jump up to:[a] [b] Vert, M.; Doi, Y.; Hellwich, K. H.; Hess, M.; Hodge, P.; Kubisa, P.; Rinaudo, M.; Schué, F. O. (2012). "Terminology for bio-related polymers and applications (IUPAC Recommendations 2012)". Pure and Applied Chemistry. 84 (2): 377 410. doi:10.1351/PAC-REC-10-12-04. S2CID 98107080.
3. Jump up to:[a] [b] Vert, Michel; Doi, Yoshiharu; Hellwich, Karl-Heinz; Hess, Michael; Hodge, Philip; Kubisa, Przemyslaw; Rinaudo, Marguerite; Schué, François (11 January 2012). "Terminology for bio-related polymers and applications (IUPAC Recommendations 2012)". Pure and Applied Chemistry. 84 (2): 377–410. doi:10.1351/PAC-REC-10-12-04. S2CID 98107080.
4. Tabebuia rosea". Germplasm Resources Information Network (GRIN). Agricultural Research Service (ARS), United States Department of Agriculture (USDA). Retrieved 15 September 2015.
5. Hernan Rodriguez Navas. 2007. La Utilidad de las Plantas Medicinales en Costa Rica. EUNA, Heredia, Costa Rica. 213pp.
6. Record, Samuel J. Lapachol. Tropical Woods (1925), 1 7-9.
7. Pai AB (2019). "Chapter 6. Iron Oxide Nanoparticle Formulations for Supplementation". In Sigel A, Freisinger E, Sigel RK, Carver PL (eds.). Essential Metals in Medicine: Therapeutic Use and Toxicity of Metal Ions in the Clinic. Metal Ions in Life Sciences. Vol. 19. Berlin: de Gruyter GmbH. pp. 157–180. doi:10.1515/9783110527872-012. ISBN 978-3-11-052691-2. PMID 30855107
8. Wang L, Hu C, Shao L. The antimicrobial activity of nanoparticles: present situation and prospects for the future. Int J Nanomedicine. 2017 Feb 14;12:1227-1249. doi: 10.2147/IJN.S121956. PMID: 28243086; PMCID: PMC5317269.
9. Parveen S, Wani AH, Shah MA, Devi HS, Bhat MY, Koka JA. Preparation, characterization, and antifungal activity of iron oxide nanoparticles. Microb Pathog. 2018 Feb;115:287-292. doi 10.1016/j.micpath.2017.12.068. Epub 2018 Jan 3. PMID: 29306005.
10. Ge X, Cao Z, Chu L. The Antioxidant Effect of the Metal and Metal-Oxide Nanoparticles. Antioxidants (Basel). 2022 Apr 18;11(4):791. doi: 10.3390/antiox11040791. PMID: 35453476; PMCID: PMC9030860.
11. E. C. Njagi, H. Huang, L. Stafford, et al., "Biosynthesis of iron and silver nanoparticles at room temperature using aqueous sorghum bran extracts," Langmuir, vol. 27, no. 1, pp. 264–271, 2011.
12. Yosmery Vitta a,⇑ , Maice Figueroa a , María Calderon b , Carlos Ciangherotti. Synthesis of iron nanoparticles from aqueous extract of Eucalyptus robusta Sm and evaluation of the antioxidant and antimicrobial activity. Materials Science for Energy Technologies 3 (2020) 97–103.
13. Ting, A. S. Y., & Chin, J. E. (2020). Biogenic synthesis of iron nanoparticles from apple peel extracts for decolorization of malachite green dye. Water, Air, & Soil Pollution, 231(6), 278.

14. Hassan Al-Karagoly*, Atiaf Rhyaf, Hala Naji, Salim Albukhaty, Faizah A. AlMalki, Amal A. Alyamani, Jawaher Albaqami, and Salman Aloufi. Green synthesis, characterization, cytotoxicity, and antimicrobial activity of iron oxide nanoparticles using Nigella sativa seed extract. Green Processing and Synthesis 2022; 11: 254–265.
15. Nahari, M.H.; Al Ali, A.; Asiri, A.; Mahnashi, M.H.; Shaikh, I.A.; Shettar, A.K.; Hoskeri, J. Green Synthesis and Characterization of Iron Nanoparticles Synthesized from Aqueous Leaf Extract of Vitex leucoxylon and Its Biomedical Applications. Nanomaterials 2022, 12, 2404. https://doi.org/10.3390/ nano12142404.
16. TheintTheint Win1,2, Sikandar Khan3, Bo Bo2, Shah Zada4 & PengCheng Fu1. Green synthesis and characterization of Fe3O4 nanoparticles using Chlorella-K01 extract for potential enhancement of plant growth stimulating and antifungal activity. Scientifc Reports | (2021) 11:21996 | https://doi.org/10.1038/s41598-021-01538-2.
17. Thiyagarajan, M., & Suriyavathana, M. (2010). Phytochemical and antimicrobial screening of Manihot escalate Crantz varieties Mulluvadi I, CO3 root bark. International Journal of Biotechnology and Biochemistry, 6(6), 859-864.
18. Sathish Kumar R, Anburaj G, Mageshkumar R, Subramanian A, Vasantha S. In vitro assessment of antioxidant and anticancer activities of Capparis zeylanica L. leaf extracts against human breast cancer (MCF-7). International Journal of Botany Studies. 6(6)1301-1305 (2021).
19. Henglein, (1993). Physicochemical properties of small metal particles in solution:" microelectrode" reactions, chemisorption, composite metal particles, and the atom-to-metal transition. The Journal of Physical Chemistry, 97(21), 5457-5471
20. Anghel, I., Grumezescu, A. M., Holban, A. M., Ficai, A., Anghel, A. G., & Chifiriuc, M. C. (2013). Biohybrid nanostructured iron oxide nanoparticles and Satureja hortensis to prevent fungal biofilm development. International journal of molecular sciences, 14(9), 18110-18123.
21. Amutha, S., & Sridhar, S. (2018). Green synthesis of magnetic iron oxide nanoparticle using leaves of Glycosmis mauritiana and their antibacterial activity against human pathogens. Journal of Innovations in Pharmaceutical and Biological Sciences, 5(2), 22-26.
22. Resale, I., Ghannadnia, M., & Baghshahi, S. (2018). Biosynthesis of silver nanoparticles using leaf extract of Satureja hortensis treated with NaCl and its antibacterial properties. Microporous and Mesoporous Materials, 264, 240-247.
23. Yu, B. Y., & Kwak, S. Y. (2010). Assembly of magnetite nanocrystals into spherical mesoporous aggregates with a 3-D wormhole-like pore structure. Journal of Materials Chemistry, 20(38), 8320-8328.
24. S. Raut, P.V Thorat, R. Thakre, Green synthesis of zinc oxide (ZnO) nanoparticles using Ocimum tenuiflorum leaves, Int. J. Sci. Res. 14 (2013) 2319–7064 (IJSR) ISSN (Online Index Copernicus Value Impact Factor.
25. S. Yedurkar, C. Maurya, P. Mahanwar, Biosynthesis of zinc oxide nanoparticles using Ixora coccinea leaf extract—a green approach, Open J. Synth. Theory Appl. 5 (2016) 1–14, doi: 10.4236/ojsta.2016.51001.
26. Aisida S.O., Madubuonu N., Alnasir M.H. Biogenic synthesis of iron oxide nanorods using Moringa oleifera leaf extract for antibacterial applications. Appl. Nanosci. 2020;10:305–315. [Google Scholar] [Ref list]
27. Liu H., Li P., Lu B., Wei Y., Sun Y. Transformation of ferrihydrite in the presence or absence of trace Fe(II): the effect of preparation procedures of ferrihydrite. J. Solid State Chem. 2009;182:1767–1771. [Google Scholar] [Ref list]
28. Qasim S., Zafar A., Saif M.S., Ali Z., Nazar M., Waqas M., Haq A.U., Tariq T., Hassan S.G., Iqbal F., Shu X.G., Hasan M. Green synthesis of iron oxide nanorods using Withania coagulans extract improved photocatalytic degradation and antimicrobial activity. J. Photochem. Photobiol. B Biol. 2020;204:111784. [PubMed] [Google Scholar] [Ref list]
29. Karpagavinayagam, P., & Vedhi, C. (2019). Green synthesis of iron oxide nanoparticles using Avicennia marina flower extract. Vacuum, 160, 286-292.
30. Sobiyana, P., Anburaj, G., & Manikandan, R. (2019). Comparative analysis of the in vitro antioxidant activity of Tabebuia rosea and Tabebuia argentea. Journal of Pharmacognosy and Phytochemistry, 8(1), 2673-2677.

31. Etsassala, N. G. E. R., Badmus, J. A., Marnewick, J. L., Iwuoha, E. I., Nchu, F., Hussein, A. A., & Egieyeh, S. (2022). Alpha-Glucosidase and Alpha-Amylase Inhibitory Activities, Molecular Docking, and Antioxidant Capacities of Plectranthus colonic Constituents. *Antioxidants*, *11*(2), 1–12. https://doi.org/10.3390/antiox11020378
32. Liu, J., Li, Q., Yang, Y., & Ma, L. (2020). Iron metabolism and type 2 diabetes mellitus: A meta-analysis and systematic review. *Journal of Diabetes Investigation*, *11*(4), 946–955. https://doi.org/10.1111/jdi.13216
33. Lu, C. H., Chen, C. C., Yu, C. S., Liu, Y. Y., Liu, J. J., Wei, S. T., & Lin, Y. F. (2022). MIB2: metal ion-binding site prediction and modeling server. *Bioinformatics (Oxford, England)*, *38*(18), 4428–4429. https://doi.org/10.1093/bioinformatics/btac534